Structure of the Roper resonance from lattice QCD constraints

Jia-jun Wu,[1] Derek B. Leinweber,[1] Zhan-wei Liu,[1,2] and Anthony W. Thomas[1,3]
[1]Special Research Centre for the Subatomic Structure of Matter (CSSM), Department of Physics, University of Adelaide, Adelaide, South Australia 5005, Australia
[2]School of Physical Science and Technology, Lanzhou University, Lanzhou 730000, China
[3]ARC Centre of Excellence for Particle Physics at the Terascale (CoEPP), Department of Physics, University of Adelaide, Adelaide, South Australia 5005, Australia

(Received 3 April 2017; published 29 May 2018)

Two different effective field theory descriptions of the pion-nucleon scattering data are constructed to describe the region of the Roper resonance. In one, the resonance is the result of strong rescattering between coupled meson-baryon channels, while in the other the resonance has a large bare-baryon (or quark-model-like) component. The predictions of these two scenarios are compared with the latest lattice QCD simulation results in this channel. We find that the second scenario is not consistent with lattice QCD results, whereas the first agrees with those constraints. In that preferred scenario, the mass of the quark-model-like state is approximately 2 GeV, with the infinite-volume Roper resonance best described as a resonance generated dynamically through strongly coupled meson-baryon channels.

DOI: 10.1103/PhysRevD.97.094509

I. INTRODUCTION

Since the discovery of the Roper resonance in 1964 [1], its peculiar properties have challenged our understanding of the quark structure of hadrons and ultimately of quantum chromodynamics (QCD) itself [2–21]. With the first negative-parity excitation of the nucleon, the $N^\star(1535)$, almost 600 MeV above the nucleon, expectations—based upon the harmonic oscillator model which has enjoyed success in treating hadron spectroscopy—suggest that the first positive-parity excited state should occur around 2 GeV. Yet, empirically one finds the first positive-parity, spin-$1/2$ Roper resonance of the nucleon to have a mass of just 1.45 GeV, *below* the $N^\star(1535)$ [22].

To make matters worse, the first negative-parity excitation of a strangeness -1 baryon, the famous $\Lambda(1405)$, is lower in mass than both of these nonstrange excited states of the nucleon [22]. Fortunately, in this case there have recently been advances in our understanding, via lattice QCD simulations of not only the mass of this state but the individual valence quark contributions to its electromagnetic form factors [23,24]. These simulations have been supported by analysis involving an effective Hamiltonian [25], which allows a natural connection to be made between the results calculated on a finite lattice volume and the infinite volume of the real world [26,27]. As a result of these studies, it is now clear that the $\Lambda(1405)$ is essentially an antikaon nucleon bound state with very little content corresponding to the sort of three-quark state anticipated in a typical quark model [24].

In this article we use similar techniques to investigate the nature of the Roper resonance. Our calculations are founded on Hamiltonian effective field theory (HEFT), an extension of chiral perturbation theory that incorporates the Lüscher relation [28–30] connecting the energy levels observed in finite volume to the scattering phase shifts [31]. In the power-counting regime, HEFT reproduces the expansion of chiral perturbation theory for ground state phenomena [32].

The results presented herein are the first to incorporate a basis state that can be associated with a quark-model state for the Roper, where radial excitations of constituent quarks describe the internal structure of the Roper. This is an important development that admits, for example, three-quark descriptions of nucleon-Roper transition form factors in the large momentum transfer regime [33] where mesonic dressings are suppressed.

The outline of this article is as follows. We first introduce the coupled-channel scattering formalism [34] in Sec. II. Experimental scattering data in the region of the Roper resonance is analyzed in Sec. III where two different descriptions of the data are obtained in the coupled-channel formalism. In the first fit there is no significant three-quark coupling, while in the second alternative fit to the data there is. These models produce rather different behavior in the unobserved $\pi\Delta$ and σN channels and cannot be distinguished by experiment. We then use the same effective field theory on a finite volume in Sec. IV to compute the spectrum one would expect to find in lattice QCD. Only the first description of the experimental data is consistent with recent lattice simulations, indicating that the Roper resonance is generated dynamically through the rescattering of coupled meson-baryon channels.

This discovery leads to a new contemporary role for constituent quark models in describing the low-lying baryon spectrum. Section V presents this role drawing on recent developments in the understanding of the odd-parity N and Λ spectra. The three-quark radial excitation of the nucleon anticipated in traditional quark models appears to lie closer to 2 GeV, which as explained earlier, is in accord with the excitation energy of the observed $N^\star(1535)$. Finally, Sec. VI summarizes our conclusions and suggests directions for future research.

II. THEORETICAL FRAMEWORK

In order to model the scattering data in the region of the Roper resonance and describe the observed inelasticity, we include three coupled channels, πN, $\pi\Delta$ and σN. In the rest frame, the Hamiltonian has the following form:

$$H = H_0 + H_I, \tag{1}$$

where the noninteracting Hamiltonian is

$$H_0 = \sum_{B_0} |B_0\rangle m_B^0 \langle B_0| + \sum_\alpha \int d^3\vec{k} |\alpha(\vec{k})\rangle [\omega_{\alpha_1}(\vec{k}) + \omega_{\alpha_2}(\vec{k})] \langle \alpha(\vec{k})|. \tag{2}$$

Here B_0 denotes a bare baryon with mass m_B^0, which may be thought of as a quark model state and α_1 (α_2) indicates the meson (baryon) state which constitutes channel α, with $\omega_{\alpha_i}(\vec{k}) = \sqrt{m_{\alpha_i}^2 + \vec{k}^2}$.

The energy independent interaction Hamiltonian includes two parts, $H_I = g + v$, where g describes the vertex interaction between the bare particle and the two-particle channels α

$$g = \sum_{\alpha, B_0} \int d^3\vec{k} \{ |\alpha(\vec{k})\rangle G^\dagger_{\alpha,B_0}(k) \langle B_0| + \text{H.c.}\}, \tag{3}$$

while the direct two-to-two particle interaction is defined by

$$v = \sum_{\alpha,\beta} \int d^3\vec{k} d^3\vec{k}' |\alpha(\vec{k})\rangle V^S_{\alpha,\beta}(k,k') \langle \beta(\vec{k}')|. \tag{4}$$

For the vertex interaction between the bare baryon and the two-particle channels we choose

$$G^2_{\alpha,B_0}(k) = \frac{g^2_{B_0\alpha}}{4\pi^2} \left(\frac{k}{f}\right)^{2l_\alpha} \frac{u^2_\alpha(k)}{\omega_{\alpha_1}(k)}, \tag{5}$$

where the pion decay constant $f = 92.4$ MeV and l_α is the orbital angular momentum in channel α. Here, since we are concerned with the Roper resonance, with isospin, angular momentum and parity, $\mathbf{I}(\mathbf{J^P}) = \frac{1}{2}(\frac{1}{2}^+)$, l is 1 for πN and $\pi\Delta$, while it is 0 for σN. The regulating form factor, $u_\alpha(k)$, takes the exponential form $u_\alpha(k) = \exp(-k^2/\Lambda_\alpha^2)$, where Λ_α is the regularization scale. For the five direct two-to-two particle interactions we introduce separable potentials

$$V^S_{\alpha,\beta}(k,k') = g^S_{\alpha,\beta} \frac{\bar{G}_\alpha(k)}{\sqrt{\omega_{\alpha_1}(k)}} \frac{\bar{G}_\beta(k')}{\sqrt{\omega_{\beta_1}(k')}}, \tag{6}$$

where $\bar{G}_\alpha(k) = G_{\alpha,B_0}(k)/g_{B_0\alpha}$. The T-matrices for two-particle scattering are obtained by solving a three-dimensional reduction of the coupled-channel Bethe-Salpeter equations for each partial wave

$$t_{\alpha,\beta}(k,k';E) = V_{\alpha,\beta}(k,k';E) + \sum_\gamma \int q^2 dq V_{\alpha,\gamma}(k,q;E) \times \frac{1}{E - \omega_{\gamma_1}(q) - \omega_{\gamma_2}(q) + i\epsilon} t_{\gamma,\beta}(q,k';E). \tag{7}$$

The coupled-channel potential is readily calculated from the interaction Hamiltonian

$$V_{\alpha,\beta}(k,k') = \sum_{B_0} \frac{G^\dagger_{\alpha,B_0}(k) G_{\beta,B_0}(k')}{E - m_B^0} + V^S_{\alpha,\beta}(k,k'), \tag{8}$$

with the normalization $\langle \alpha(\vec{k})|\beta(\vec{k}')\rangle = \delta_{\alpha,\beta}\delta(\vec{k} - \vec{k}')$. The pole position of any bound state or resonance is obtained by searching for the poles of the T-matrix in the complex plane.

In order to compare the predictions of this infinite-volume model with the results of lattice QCD simulations, it is necessary to rewrite the problem on a finite volume. The details of this procedure are described in Refs. [25,26,31,34–36]. By solving for the eigenstates of the HEFT one obtains energy levels and eigenstates which can be compared with the energies and interpolating fields in the lattice QCD simulations.

We can also extend the formalism to unphysical pion masses. Using m_π^2 as a measure of the light quark masses, we consider the variation of the bare mass and σ-meson mass as

$$m_B^0(m_\pi^2) = m_B^0|_{\text{phy}} + \alpha_B^0(m_\pi^2 - m_\pi^2|_{\text{phy}}), \tag{9}$$

$$m_\sigma^2(m_\pi^2) = m_\sigma^2|_{\text{phy}} + \alpha_\sigma^0(m_\pi^2 - m_\pi^2|_{\text{phy}}), \tag{10}$$

where the slope parameter α_B^0 is constrained by lattice QCD data from the CSSM. In the large quark mass regime, where constituent quark degrees of freedom become relevant, one expects [37] $\alpha_\sigma^0 = (2/3)\alpha_N^0$. The nucleon and Delta masses away from the physical point are obtained via linear interpolation between the lattice QCD results.

The incorporation of couplings between the three scattering channels requires 6 parameters and coupling of these channels to a bare basis state requires another three. Regularization admits four fit parameters. This description is typical of contemporary analyses of resonance phenomena [38–40] and ensures accuracy in connecting experiment to the finite-volume spectrum.

III. EXPERIMENTAL DATA ANALYSIS

By fitting the experimental data for πN scattering from 1200 to 1800 MeV, we found two different parameter sets which appear equally acceptable in describing existing data. The phase shifts and inelasticities for the $\pi N \to \pi N$ channel are shown for these two scenarios in Fig. 1. The parameter sets are described in Table I. The χ^2 for scenarios I and II are 241 and 135 respectively. The larger χ^2 for scenario I has its origin in just 6 points at the opening of the $\pi\Delta$ channel and can be attributed to the zero-width approximation for the Δ. In the context of the benchmark result [41] of $\chi^2 = 236$, both fits may be regarded as an acceptable characterization of the experimental data.

In scenario I, the coupling of $\pi N \to \pi N$ is enhanced while the coupling of the bare state to πN and σN is suppressed relative to scenario II. This presents two different pictures of the Roper. In scenario I, the Roper is a resonance generated by strong rescattering in the meson-baryon channels. In scenario II the rescattering is weaker and the observed resonance is dominated by coupling to an underlying bare, or quark-model-like, state. It is this latter scenario that the community has anticipated for the Roper since the advent of the constituent quark model [2].

While both scenarios describe the present experimental data, they make unique predictions in the coupled channels $\pi\Delta \to \pi\Delta$ and $\sigma N \to \sigma N$ as illustrated in Fig. 2. Measurements of these scattering amplitudes would enable us to distinguish between the scenarios.

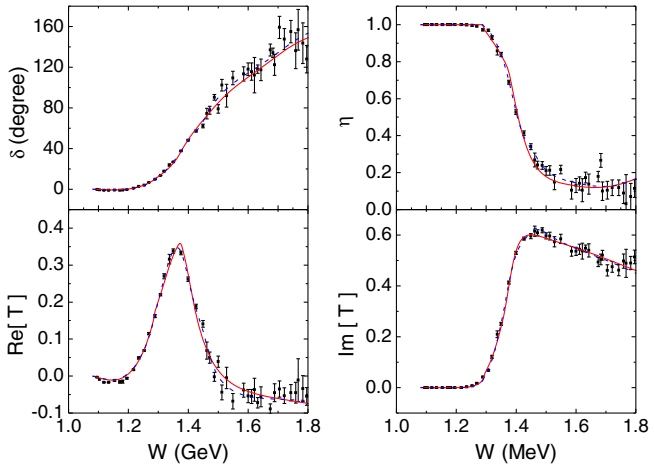

FIG. 1. The fitted phase shift δ, inelasticity η and T-matrix for the $\pi N \to \pi N$ reaction. Red-solid and blue-dashed lines are calculated from scenarios I and II, respectively.

TABLE I. Fit parameters constrained by πN scattering data and the resultant pole positions in the two scenarios described in the text. The pole position in the different Riemann sheets is also indicated for each channel (πN, $\pi\Delta$, σN). The unphysical sheet is denoted "u" and the physical sheet is denoted "p," as defined in Ref. [42,43].

Parameter	I	II
$g^S_{\pi N,\pi N}$	1.156	0.634
$g^S_{\pi N,\pi\Delta}$	−0.662	−0.378
$g^S_{\pi N,\sigma N}$	−0.415	−1.738
$g^S_{\pi\Delta,\pi\Delta}$	−0.438	−0.581
$g^S_{\pi\Delta,\sigma N}$	1.332	0.964
$g^S_{\sigma N,\sigma N}$	10.000	10.000
m^0_B/GeV	2.000	1.7000
$g_{B_0\pi N}$	0.268	0.954
$g_{B_0\pi\Delta}$	1.544	−0.118
$g_{B_0\sigma N}$	⋯	−2.892
$\Lambda_{\pi N}$/GeV	0.5953	0.6302
$\Lambda_{\pi\Delta}$/GeV	1.5000	1.4318
$\Lambda_{\sigma N}$/GeV	1.5000	1.4533
Pole (MeV) (uuu)	2012.28–42.09i	1355.57–70.81i
Pole (MeV) (upu)	1392.92–167.13i	1362.33–100.53i

IV. LATTICE QCD CONSTRAINTS

In the absence of the relevant experimental data, we now turn to the results provided by lattice QCD simulations, focusing on the recent work of Lang *et al.* [44] and the CSSM [34]. HEFT predictions in the finite volume of the

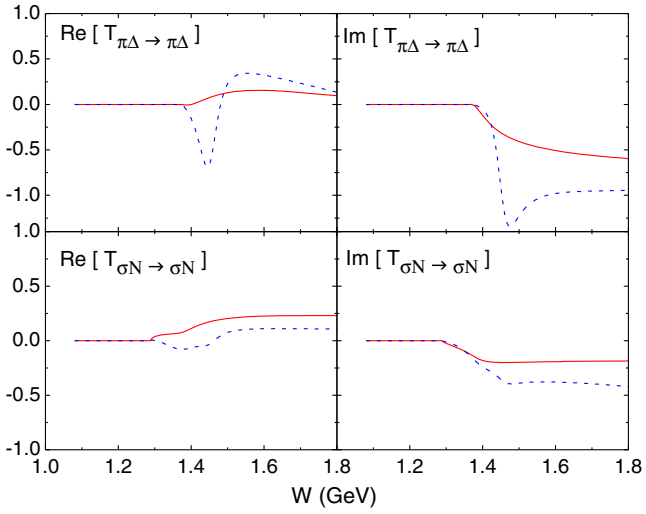

FIG. 2. The T-matrices for $\pi\Delta \to \pi\Delta$ and $\sigma N \to \sigma N$ corresponding to the two scenarios described in the text. The two cases are encoded as in Fig. 1 where red-solid and blue-dashed lines are calculated from scenarios I and II, respectively.

lattice are constrained at the physical quark masses by the fit to experimental data. To extend the predictions to other quark masses, we introduce one new parameter, α_B^0 of Eq. (9), providing a linear quark-mass dependence in the bare mass. Noting that the lattice simulation at the lightest quark mass involves a pion mass of 156 MeV, our key results are insensitive to this extension to larger pion masses.

Lang *et al.*'s work [44] is particularly interesting as it incorporates πN and σN five-quark nonlocal interpolating fields with the momenta of each hadron projected to provide excellent overlap with the low-lying scattering states of the spectrum. These results are particularly important in discriminating between scenarios I and II.

These nonlocal interpolators are complemented by standard local three-quark interpolating fields, which have proved to favor localized states and miss the nonlocal scattering states [45–50], making the lattice spectrum incomplete. In this case there may be concern that the lattice energy levels extracted might be systematically contaminated from the missed levels. The CSSM Collaboration has explored this in detail [48–50] and has developed methods that ensure these systematic errors are suppressed through Euclidean time evolution. Their use of a single-state ansatz and a full covariance-matrix calculation of the χ^2/d.o.f. with a conservative cutoff of $\chi^2/\text{d.o.f.} < 1.2$ ensures that any remaining contamination is contained within the error bars reported [50]. While the resultant uncertainties overlap with several states in the HEFT spectrum, we will see that it is the absence of localized states below 1.9 GeV [50,51] that facilitates a discrimination of scenarios I and II.

In reporting the lattice QCD results in Figs. 3 and 4 we have used solid (open) symbols to indicate states dominated by local (nonlocal) interpolating fields. While the operator overlaps are unrenormalized matrix elements and therefore scale dependent, the qualitative aspects of this information can be used to gain insight into the composition of the states in addition to the standard analysis of the spectrum. Just as insight into the composition of the lattice QCD states can be obtained from the eigenvectors of the lattice correlation matrix used to excite the states, HEFT also provides insight into their composition via the superposition of basis states in each eigenvector.

Bär [52] has shown that the overlap of the noninteracting nonlocal πN channel with standard local three-quark interpolating fields is suppressed by 3 orders of magnitude relative to the ground state nucleon on a 3 fm lattice. Thus the lattice QCD states that are excited by local three-quark operators correspond to HEFT states having a significant bare-basis-state component in their eigenvector. This information is indicated through the color coding of the HEFT spectra illustrated in Figs. 3 and 4 for scenarios I and II respectively. The red, blue, green and orange lines indicate the states having the first, second, third and fourth largest bare-baryon basis-state contributions, respectively.

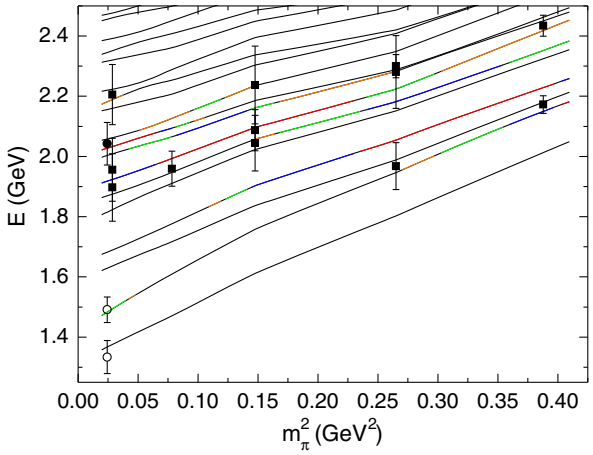

FIG. 3. The finite volume spectrum of scenario I with a bare mass of 2.0 GeV. The CSSM results [34] are indicated by square symbols and circles denote the more recent results from Lang *et al.* [44]. Solid symbols indicate states dominated by local three-quark operators and open symbols indicate states dominated by nonlocal momentum-projected five-quark operators. The colors red, blue, green and orange are used to indicate the relative contributions of the bare-baryon basis state in the eigenstate, with red being the largest contribution.

For scenario I of Fig. 3, all of the lattice states dominated by local three-quark interpolating fields can be associated with a colored line. Similarly, all of the Hamiltonian states having the largest bare basis-state component, indicated in red in Fig. 3, have a nearby lattice QCD result. We quantify this agreement through a χ^2 measure associating each three-quark dominated (solid) lattice point with a three-quark dominated HEFT state. Open symbols are associated with the nearest HEFT level. For scenario I the minimum $\chi^2/\text{d.o.f.} = 16.5/(15–1) = 1.18$.

On the other hand, scenario II of Fig. 4 displays little correspondence to the lattice QCD results. Scenario II

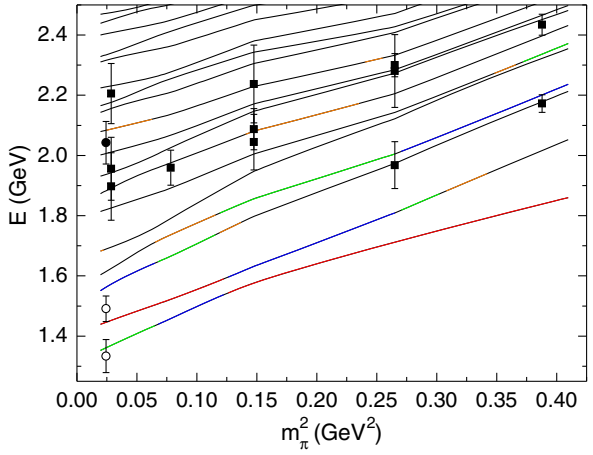

FIG. 4. The finite volume spectrum corresponding to scenario II having a bare mass of 1.7 GeV. Results are illustrated as described in Fig. 3.

predicts a low-lying state with a large bare basis-state component of approximately 50%, approaching that for the ground state. Such a state would be easy to excite in lattice QCD with local three-quark operators. However this three-quark dominated state is not seen in the simulations. For this scenario, the χ^2 measure provides $\chi^2/\text{d.o.f.} = 635.7/(15–1) = 45.4$.

We also consider a simple χ^2 measure where only the most bare-state dominated HEFT state and the closest three-quark-interpolator dominated lattice QCD point are considered at each mass. In scenario I the $\chi^2/\text{d.o.f.} = 5.78/(6–1) = 1.16$, whereas in scenario II the $\chi^2/\text{d.o.f.} = 338/(6–1) = 68$.

Focusing now on the lattice QCD results from Lang *et al.* [44] at near physical quark masses, we see that both the energy levels and their composition are correctly described in scenario I of Fig. 3. The lowest-lying lattice QCD state appears with the introduction of their momentum-projected σN interpolator. The second state disappears if their momentum-projected πN interpolator is omitted [44]. This composition agrees with the composition predicted by HEFT in scenario I reported in Fig. 5. Near the physical mass the first eigenstate is dominated by σN basis states. The second state is dominated by the πN channel complemented by some mixing with $\pi\Delta$.

While the HEFT of scenario I correctly describes the composition of these states, scenario II describes the lattice πN state as a three-quark dominated state with 50% of the composition in the local three-quark state. Yet three-quark interpolators do not see this state. This is an important discrepancy which again excludes scenario II as an acceptable description of the nucleon spectrum.

It is only for the seventh, eighth and ninth eigenstates of scenario I that we find a significant bare basis-state contribution in Fig. 5 and this is precisely where the lattice QCD states excited by local three-quark operators reside. The ninth state has an extremely large bare-state component exceeding 50% and both the CSSM and Lang *et al.* observe three-quark dominated lattice QCD eigenstates within one sigma of this state, lending further credence to scenario I as the correct description of the nucleon spectrum.

Finally, we examine how the eigenstates evolve as the pion mass increases. In Fig. 5 we see that in scenario I, the bare-baryon content of the second and fourth eigenstates increases towards the upper end of the pion-mass range. Once again this is consistent with the lattice simulations as this is where the CSSM finds lower mass states in the spectrum with local three-quark operators. Overall the Hamiltonian eigenvectors obtained within scenario I explain the lattice spectra very well.

In contrast, the lowest-mass eigenstates of scenario II are dominated by the bare-baryon basis state. At near-physical quark masses, their composition is inconsistent with the results of Lang *et al.* and at larger quark masses neither the CSSM nor the Cyprus Collaboration [53] observed such low-lying states in their 3 fm lattice results.

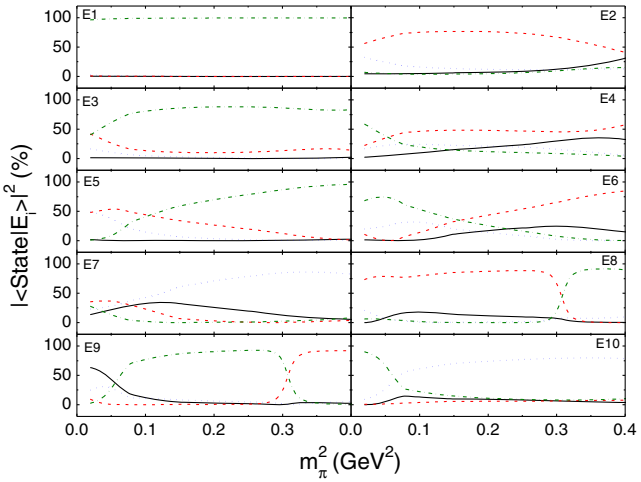

FIG. 5. The pion-mass evolution of the Hamiltonian eigenvector components for scenario I having a bare mass of 2.0 GeV. The black solid line indicates the fraction of the bare state, $|\langle m_0|E_i\rangle|^2$. The red-dashed, blue-dotted and green dashed-dotted lines show the πN, $\pi\Delta$ and σN "state" contributions to the energy eigenstate $|E_i\rangle$ respectively, summed over all discrete momenta, $\sum_{\vec{k}}|\langle\alpha(\vec{k})|E_i\rangle|^2$. The labels "Ei" indicate the i-th energy level.

V. CONTEMPORARY ROLE FOR THE QUARK MODEL

Through a consolidation of the earlier lattice QCD and HEFT approaches to the study of the $N^*(1535)$ and $\Lambda^*(1405)$ resonances and the study of the $N^*(1440)$ resonance herein, a new understanding of the nature of these resonances and the role of the quark model is emerging.

(1) The $N^*(1535)$ is dominated by a three-quark core and dressed by a meson cloud [25]. While the role of the meson cloud is enhanced, the structure of this state is qualitatively similar to ground state.

(2) The $\Lambda^*(1405)$ is predominantly a molecular $\bar{K}N$ bound state [23,26]. Mixing with the $\pi\Sigma$ channel creates a resonance with a two-pole structure. The excited state of the quark model lies higher at approximately 1.6 GeV.

(3) The $N^*(1440)$ resonance is best described as the result of strong rescattering between coupled meson-baryon channels with only a small component associated with a quark-model-like state. This small but nontrivial contribution is indicated by the green curve in Fig. 3 through the second excitation reported by Lang *et al.* [44]. The first radially excited nucleon of the quark model has a mass of approximately 2 GeV.

These conclusions provide a new understanding of the low-lying N and Λ resonances as illustrated in Fig. 6. With regard to the simple constituent quark model, we now understand that it predicts three levels of hadron mass with

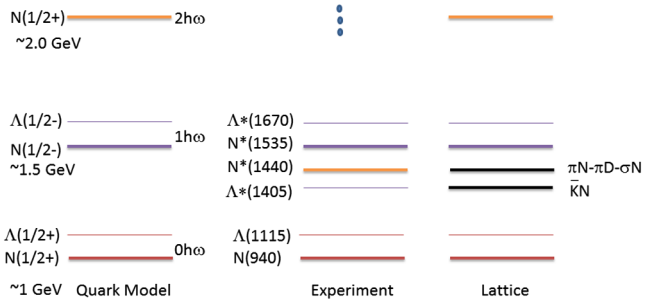

FIG. 6. The low-lying N and Λ spectra of the simple quark model described herein are presented in the context of experimental data and the results of lattice QCD plus HEFT analyses as described in the text.

approximately equal spacings. It describes the ground state, an odd-parity state the order of 500 MeV above the ground state and an even parity excitation approximately 1 GeV above the ground state.

Within the context of a constituent quark model, a mass of 2 GeV for the first radial excitation is natural. With the first negative-parity excitation of the nucleon, the $N^\star(1535)$, approximately 500 MeV above the nucleon, expectations—based upon a phenomenologically successful harmonic oscillator model—suggest that the first positive-parity excited state should occur another 500 MeV above, at around 2 GeV.

We now understand that the structure of the $\Lambda^*(1405)$ and $N^*(1440)$ is more complicated and beyond the scope of a simple model based on three constituent quarks. Through the analyses of lattice QCD results with HEFT, the nature of the $\Lambda^*(1405)$ and $N^*(1440)$ appears to be predominantly meson-baryon states. In other words, these two states are beyond the quark model and tuning quark model parameters to encompass these states spoils the insight to be gained from these models. Indeed, the states predicted in the quark model as discussed above, are observed in the spectra of contemporary lattice QCD results.

VI. CONCLUSION

We have examined experimental pion-nucleon scattering data in Hamiltonian effective field theory, an extension of chiral perturbation theory that incorporates the Lüscher relation connecting the scattering phase shifts to the energy levels observed in finite volume lattice QCD calculations. By considering the Hamiltonian matrix in the finite-volume, one not only learns the energy eigenvalues corresponding to the spectrum of lattice QCD simulations, but one also learns the eigenvectors of these eigenstates describing the composition of the states. This information has been key to advancing our understanding of the structure of low-lying baryon resonances.

We developed two scenarios for describing the Roper resonance in the pion-nucleon scattering process. Scenario I describes the Roper resonance as a baryon-meson scattering state, while scenario II describes the Roper as a traditional three-quark state. Both scenarios can fit the experimental data very well. However, only scenario I is consistent with lattice QCD results.

A particular focus of this investigation has been to ascertain the possible role of a basis state in the Hamiltonian formulation that can be associated with a quark-model-like radial excitation of the nucleon. In conclusion, the quark-model-like basis state associated with the Roper resonance lies at approximately 2 GeV. This large mass is required in order to provide a finite-volume spectrum consistent with lattice QCD. A lower bare-basis-state mass leads to the prediction of quark-model-like low-lying states dominated by a bare-state component. The absence of such states in the lattice QCD spectrum rules out this scenario.

The description of both the experimental scattering data in Fig. 1 and the lattice results presented in Fig. 3 for this scenario is excellent. All localized lattice QCD states are associated with a HEFT spectral line whose composition includes a large quark-model-like basis state component. Similarly, HEFT accurately predicts the positions of the scattering states observed in lattice QCD by Lang *et al.* [44] as well as their composition.

In the preferred scenario I with a 2 GeV bare-state mass, quark-model-like states sit high in the spectrum. In the finite volume of the $L = 3$ fm lattice, the bare state is dressed to produce states commencing at $\simeq$1.9 GeV for the lightest pion mass of 156 MeV. Indeed, the CSSM studied the three-quark wave function of this state and discovered it resembles the first radial excitation of the quark model [54,55]. In the infinite volume, this state is associated with a pole at approximately 2 GeV.

Thus, it is now clear that there is an unconventional role for a quark-model-like description of the Roper in describing experimental data and the lattice QCD results. The analysis shows that one can admit such a state provided it sits high in the spectrum at approximately 2 GeV. Remarkably, this is where simple quark models naturally place the radial excitation of the nucleon.

Even though there are no localized states seen on the lattice between this energy scale of $\simeq$1.9 GeV and the ground state nucleon mass [50], scenario I generates an infinite-volume pole in the Roper resonance region of the spectrum. This pole arises from strong rescattering in the coupled meson-baryon channels, which dominate the underlying structure of the Roper resonance.

These conclusions reveal that the spectrum of quark-model-like states is relatively simple, once one excludes the more exotic $\Lambda^*(1405)$ and $N^*(1440)$ from the traditional scope of the model. The $\Lambda^*(1405)$ and $N^*(1440)$ contain nontrivial meson-baryon interactions with the $\Lambda^*(1405)$ dominated by a molecular $\bar{K}N$ component and the $N^*(1440)$ arising out of strong meson-baryon rescattering.

Finally, the relationship between the radial excitation of the nucleon and the Roper resonance is now understood.

The quark-model-like basis state at approximately 2 GeV makes a small but nontrivial contribution to the finite volume state observed in the regime of the Roper resonance by Lang *et al.* at $\simeq 1.5$ GeV. While this state is excited with the momentum-projected σN interpolating field, it has a small 2 GeV quark-model-like basis-state component in HEFT, as indicated by the green curve in Fig. 3 through the second excitation reported by Lang *et al.* [44]. This component may become the dominant component in large Q^2 transition form factors [33] where long-distance meson-cloud effects are highly suppressed. Still, the predominant structure of the Roper resonance has its origin in the strong rescattering of πN, $\pi\Delta$ and σN channels.

With this new insight, the mystery of the low-lying Roper resonance may be nearing resolution. Evidence indicates the observed nucleon resonance at 1440 MeV is best described as the result of strong rescattering between coupled meson-baryon channels.

In working towards a definitive analysis there is ample scope for new data to further resolve the nature of this state. Further development of three-body channel contributions [56,57] in effective field theory is desired. Similarly, a more comprehensive lattice QCD analysis of the *complete* nucleon spectrum in several lattice volumes would serve well to further expose the role of the coupled channels giving rise to the Roper resonance.

ACKNOWLEDGMENTS

This research was supported by the Fundamental Research Funds of Lanzhou University under Grant No. 223000-862637 and by the Australian Research Council through the ARC Centre of Excellence for Particle Physics at the Terascale (CE110001104) and through Grants No. DP151103101 (A. W. T.), No. DP140103067 and No. DP150103164 (D. B. L.).

[1] L. D. Roper, Phys. Rev. Lett. **12**, 340 (1964).
[2] N. Isgur and G. Karl, Phys. Rev. D **19**, 2653 (1979); **23**, 817 (E) (1981).
[3] I. G. Aznauryan *et al.* (CLAS Collaboration), Phys. Rev. C **78**, 045209 (2008).
[4] K. Joo *et al.* (CLAS Collaboration), Phys. Rev. C **72**, 058202 (2005).
[5] H. J. Weber, Phys. Rev. C **41**, 2783 (1990).
[6] B. Julia-Diaz and D. O. Riska, Nucl. Phys. **A780**, 175 (2006).
[7] D. Barquilla-Cano, A. J. Buchmann, and E. Hernandez, Phys. Rev. C **C75**, 065203 (2007); **77**, 019903(E) (2008).
[8] B. Golli and S. Sirca, Eur. Phys. J. A **38**, 271 (2008).
[9] B. Golli, S. Sirca, and M. Fiolhais, Eur. Phys. J. A **42**, 185 (2009).
[10] U. G. Meissner and J. W. Durso, Nucl. Phys. **A430**, 670 (1984).
[11] C. Hajduk and B. Schwesinger, Phys. Lett. **140B**, 172 (1984).
[12] O. Krehl, C. Hanhart, S. Krewald, and J. Speth, Phys. Rev. C **62**, 025207 (2000).
[13] C. Schutz, J. Haidenbauer, J. Speth, and J. W. Durso, Phys. Rev. C **57**, 1464 (1998).
[14] A. Matsuyama, T. Sato, and T. S. H. Lee, Phys. Rep. **439**, 193 (2007).
[15] H. Kamano, S. X. Nakamura, T. S. H. Lee, and T. Sato, Phys. Rev. C **81**, 065207 (2010).
[16] H. Kamano, S. X. Nakamura, T. S. H. Lee, and T. Sato, Phys. Rev. C **88**, 035209 (2013).
[17] N. Suzuki, B. Julia-Diaz, H. Kamano, T. S. H. Lee, A. Matsuyama, and T. Sato, Phys. Rev. Lett. **104**, 042302 (2010).
[18] E. Hernandez, E. Oset, and M. J. Vicente Vacas, Phys. Rev. C **66**, 065201 (2002).
[19] T. Barnes and F. E. Close, Phys. Lett. **123B**, 89 (1983).
[20] E. Golowich, E. Haqq, and G. Karl, Phys. Rev. D **28**, 160 (1983); **33**, 859(E) (1986).
[21] L. S. Kisslinger and Z. P. Li, Phys. Rev. D **51**, R5986 (1995).
[22] C. Patrignani *et al.* (Particle Data Group), Chin. Phys. C **40**, 100001 (2016).
[23] J. M. M. Hall, W. Kamleh, D. B. Leinweber, B. J. Menadue, B. J. Owen, A. W. Thomas, and R. D. Young, Phys. Rev. Lett. **114**, 132002 (2015).
[24] J. M. M. Hall, W. Kamleh, D. B. Leinweber, B. J. Menadue, B. J. Owen, and A. W. Thomas, Phys. Rev. D **95**, 054510 (2017).
[25] Z.-W. Liu, W. Kamleh, D. B. Leinweber, F. M. Stokes, A. W. Thomas, and J.-J. Wu, Phys. Rev. Lett. **116**, 082004 (2016).
[26] Z.-W. Liu, J. M. M. Hall, D. B. Leinweber, A. W. Thomas, and J.-J. Wu, Phys. Rev. D **95**, 014506 (2017).
[27] R. Molina and M. Döring, Phys. Rev. D **94**, 056010 (2016); **94**, 079901(E) (2016).
[28] M. Luscher, Commun. Math. Phys. **105**, 153 (1986).
[29] M. Luscher, Nucl. Phys. **B354**, 531 (1991).
[30] M. Luscher, Nucl. Phys. **B364**, 237 (1991).
[31] J.-J. Wu, T. S. H. Lee, A. W. Thomas, and R. D. Young, Phys. Rev. C **90**, 055206 (2014).
[32] R. D. Young, D. B. Leinweber, and A. W. Thomas, Prog. Part. Nucl. Phys. **50**, 399 (2003).
[33] D. J. Wilson, I. C. Cloet, L. Chang, and C. D. Roberts, Phys. Rev. C **85**, 025205 (2012).
[34] Z.-W. Liu, W. Kamleh, D. B. Leinweber, F. M. Stokes, A. W. Thomas, and J.-J. Wu, Phys. Rev. D **95**, 034034 (2017).
[35] J. M. M. Hall, A. C. P. Hsu, D. B. Leinweber, A. W. Thomas, and R. D. Young, Phys. Rev. D **87**, 094510 (2013).

[36] J.-J. Wu, H. Kamano, T. S. H. Lee, D. B. Leinweber, and A. W. Thomas, Phys. Rev. D **95**, 114507 (2017).
[37] I. C. Cloet, D. B. Leinweber, and A. W. Thomas, Phys. Rev. C **65**, 062201 (2002).
[38] B. Julia-Diaz, T. S. H. Lee, A. Matsuyama, and T. Sato, Phys. Rev. C **76**, 065201 (2007).
[39] R. A. Arndt, W. J. Briscoe, I. I. Strakovsky, and R. L. Workman, Phys. Rev. C **74**, 045205 (2006).
[40] D. Ronchen, M. Doring, F. Huang, H. Haberzettl, J. Haidenbauer, C. Hanhart, S. Krewald, U. G. Meissner, and K. Nakayama, Eur. Phys. J. A **49**, 44 (2013).
[41] GW Data Analysis Center, Institute for Nuclear Studies, The George Washington University, http://gwdac.phys.gwu.edu/analysis/pin_analysis.html.
[42] N. Suzuki, T. Sato, and T. S. H. Lee, Phys. Rev. C **79**, 025205 (2009).
[43] M. Doring, C. Hanhart, F. Huang, S. Krewald, and U. G. Meissner, Nucl. Phys. **A829**, 170 (2009).
[44] C. B. Lang, L. Leskovec, M. Padmanath, and S. Prelovsek, Phys. Rev. D **95**, 014510 (2017).
[45] M. S. Mahbub, W. Kamleh, D. B. Leinweber, P. J. Moran, and A. G. Williams (CSSM Lattice Collaboration), Phys. Lett. B **707**, 389 (2012).
[46] M. S. Mahbub, W. Kamleh, D. B. Leinweber, P. J. Moran, and A. G. Williams, Phys. Rev. D **87**, 011501 (2013).
[47] M. S. Mahbub, W. Kamleh, D. B. Leinweber, P. J. Moran, and A. G. Williams, Phys. Rev. D **87**, 094506 (2013).
[48] M. S. Mahbub, W. Kamleh, D. B. Leinweber, and A. G. Williams, Ann. Phys. (Amsterdam) **342**, 270 (2014).
[49] A. L. Kiratidis, W. Kamleh, D. B. Leinweber, and B. J. Owen, Phys. Rev. D **91**, 094509 (2015).
[50] A. L. Kiratidis, W. Kamleh, D. B. Leinweber, Z.-W. Liu, F. M. Stokes, and A. W. Thomas, Phys. Rev. D **95**, 074507 (2017).
[51] J. J. Dudek and R. G. Edwards, Phys. Rev. D **85**, 054016 (2012).
[52] O. Bär, Int. J. Mod. Phys. A **32**, 1730011 (2017).
[53] C. Alexandrou, T. Leontiou, C. N. Papanicolas, and E. Stiliaris, Phys. Rev. D **91**, 014506 (2015).
[54] D. S. Roberts, W. Kamleh, and D. B. Leinweber, Phys. Lett. B **725**, 164 (2013).
[55] D. S. Roberts, W. Kamleh, and D. B. Leinweber, Phys. Rev. D **89**, 074501 (2014).
[56] M. T. Hansen and S. R. Sharpe, Phys. Rev. D **90**, 116003 (2014).
[57] M. T. Hansen and S. R. Sharpe, Phys. Rev. D **92**, 114509 (2015).